

# An Empirical Correction for Activity Effects on the Temperatures, Radii, and Estimated Masses of Low-Mass Stars and Brown Dwarfs

Keivan G. Stassun<sup>1,2</sup>, Kaitlin M. Kratter<sup>3</sup>, Aleks Scholz<sup>4</sup>, and Trent J. Dupuy<sup>3,5</sup>

## ABSTRACT

We present empirical relations for determining the amount by which the effective temperatures and radii—and therefore the estimated masses—of low-mass stars and brown dwarfs are altered due to chromospheric activity. We base our relations on a large set of low-mass stars in the field with H $\alpha$  activity measurements, and on a set of low-mass eclipsing binaries with X-ray activity measurements from which we indirectly infer the H $\alpha$  activity. Both samples yield consistent relations linking the amount by which an active object’s temperature is suppressed, and its radius inflated, to the strength of its H $\alpha$  emission. These relations are found to approximately preserve bolometric luminosity. We apply these relations to the peculiar brown-dwarf eclipsing binary 2M0535–05, in which the active, higher-mass brown dwarf has a cooler temperature than its inactive, lower-mass companion. The relations correctly reproduce the observed temperatures and radii of 2M0535–05 after accounting for the H $\alpha$  emission; 2M0535–05 would be in precise agreement with theoretical isochrones were it inactive. The relations that we present are applicable to brown dwarfs and low-mass stars with masses below  $0.8 M_{\odot}$  and for which the activity, as measured by the fractional H $\alpha$  luminosity, is in the range  $-4.6 \lesssim \log L_{\text{H}\alpha}/L_{\text{bol}} \lesssim -3.3$ . We expect these relations to be most useful for correcting radius and mass estimates of low-mass stars and brown dwarfs over their active lifetimes (few Gyr) and when the ages or distances (and therefore luminosities) are unknown. We also discuss the implications of this work for improved determinations of young cluster initial mass functions.

*Subject headings:* stars: low-mass, brown dwarfs — stars: fundamental parameters — stars: activity

## 1. Introduction

Observational evidence strongly indicates that the fundamental properties of low-mass stars can be altered in the presence of strong magnetic activity (e.g. Morales et al. 2008; López-Morales 2007; Ribas 2006). In particular, observations of numerous active, low-mass eclipsing binary (EB) stars have found the empirically measured stellar radii ( $R$ ) to be inflated by  $\approx 10\%$ , and the empirically measured stellar effective temperatures ( $T_{\text{eff}}$ ) to be suppressed by  $\approx 5\%$ , relative to the predictions of standard theoretical stellar evolution models, which better match the properties of inactive objects (see Coughlin et al. 2011; Kraus et al.

---

<sup>1</sup>Department of Physics & Astronomy, Vanderbilt University, Nashville, TN 37235, USA. keivan.stassun@vanderbilt.edu

<sup>2</sup>Department of Physics, Fisk University, Nashville, TN 37208, USA

<sup>3</sup>Harvard-Smithsonian Center for Astrophysics, 60 Garden Street, Cambridge, MA 02138, USA

<sup>4</sup>School of Cosmic Physics, Dublin Institute for Advanced Studies, 31 Fitzwilliam Place, Dublin 2, Ireland

<sup>5</sup>Hubble Fellow

2011; Morales et al. 2010; Torres et al. 2010, and references therein). Because the mass-radius and mass- $T_{\text{eff}}$  relationships are central to our understanding of stellar evolution, resolving these discrepancies will be critical to the ongoing development of accurate theoretical stellar models (for a discussion, see Stassun et al. 2010). Accurate estimates of stellar radii are especially important in the context of searches for transiting exoplanets, which rely upon the assumed stellar radius/density to infer the planet radius/density.

Activity effects also lead to errors in object masses ( $M$ ) when these are derived from  $T_{\text{eff}}$ . A particularly salient example is 2M0535–05, an EB in the Orion Nebula Cluster (age  $\sim 1$  Myr) comprising two brown dwarfs (Stassun et al. 2006, 2007). The primary and secondary brown dwarf (BD) components of 2M0535–05 have dynamically measured masses of  $60 \pm 3$  and  $39 \pm 2$   $M_{\text{Jup}}$ , respectively, and  $T_{\text{eff}}$  ratio of  $T_1/T_2 = 0.952 \pm 0.004$  (Gómez Maqueo Chew et al. 2009). That is, the system exhibits a reversal of the usual  $M$ - $T_{\text{eff}}$  relation, such that the primary component is cooler than its companion. This behavior is not predicted by theoretical models for coeval BDs. Figure 1 shows the 2M0535–05 system on the Hertzsprung-Russell (H-R) diagram compared to the 1 Myr isochrone of Baraffe et al. (1998). The secondary BD’s  $T_{\text{eff}}$  and bolometric luminosity ( $L_{\text{bol}}$ , calculated directly from the empirically measured  $T_{\text{eff}}$  and  $R$ ) place it at a position that is consistent with that predicted by the model isochrone. In contrast, the primary is far displaced from its expected position, and so *appears* to have a mass of only  $\sim 25$   $M_{\text{Jup}}$ —more than a factor of 2 lower than its true mass—on the basis of its low  $T_{\text{eff}}$ . Reiners et al. (2007) used spectrally resolved  $H\alpha$  measurements to show that, whereas the secondary BD in 2M0535–05 is chromospherically quiet, the primary BD is highly chromospherically active, perhaps a consequence of its rapid rotation (Gómez Maqueo Chew et al. 2009). Thus, magnetic activity in the primary BD could be responsible for its highly suppressed  $T_{\text{eff}}$ , similar to what has been seen for low-mass stellar EBs in the field.

Given the exhibition of activity-related  $T_{\text{eff}}$  suppression in 2M0535–05, the first and only EB containing an active BD, it is likely that this phenomenon extends to other active BDs and low-mass stars in star forming regions and in the field. This has important implications for estimating masses from the H-R diagram, as is often necessary at the youngest ages. When the distance of a low-mass main-sequence star is known, mass can be estimated from its luminosity either via empirical mass-magnitude relations or model mass- $L_{\text{bol}}$  relations, circumventing the need to use  $T_{\text{eff}}$ . However, the use of luminosities can be problematic for very young objects, because they are sensitive to age, accretion, disk excess, and extinction—although careful evaluation of these parameters can mitigate these problems (e.g., Da Rio et al. 2012). For low-mass stars,  $T_{\text{eff}}$ -derived parameters are useful on the pre-main-sequence, during which they evolve along nearly vertical tracks on the H-R diagram, and also while they remain active on the main-sequence lifetime. The activity timescale is relatively short at higher masses ( $\lesssim 1$  Gyr for spectral types  $\leq M2$ ) but increases substantially at lower masses ( $\gtrsim 7$  Gyr for spectral types M5–M7) (West et al. 2008). For substellar objects, determining physical properties is more complicated because such objects never reach a stable main sequence. Even with an accurately known distance and thus  $L_{\text{bol}}$ , the mass and age will be degenerate. Thus, mass estimates for field BDs are generally inaccessible in the absence of age information. At the youngest ages ( $\lesssim 100$  Myr) the mass- $L_{\text{bol}}$  relationship for BDs is substantially flatter as they are still undergoing significant contraction of their radii, so the situation is more akin to pre-main-sequence stars where it is important to know  $T_{\text{eff}}$  accurately. These evolutionary phases are also when BDs are most active, unlike at field ages when they have reached spectral types  $\gtrsim L4$  for which activity is very rarely observed (e.g. Burgasser et al. 2002).

Since magnetic activity seems to alter the fundamental properties of both stars and BDs, it would be valuable to have an easily observable empirical metric with which to quantitatively assess the degree to which a given object’s  $T_{\text{eff}}$  has been suppressed and its radius inflated. In the absence of a detailed understanding of the underlying physical causes of this effect, such a metric would be a useful “stop-gap”—it mitigates one

source of uncertainty in estimates of fundamental parameters for very low mass objects. The desired metric will allow us to compare magnetically active objects with their inactive counterparts and with non-magnetic evolutionary tracks in order to improve the mass estimates for young low-mass stars and BDs.

The aim of this paper is to derive such an empirical metric by relating the degree of  $T_{\text{eff}}$  suppression and radius inflation to the strength of the  $\text{H}\alpha$  emission line, a commonly used and readily observable tracer of chromospheric activity (Scholz et al. 2007; Berger 2006). A challenge with any activity-based measure is that most active objects exhibit variability in their activity levels, and the amplitude of this variability can in some cases be quite large. For example, Bell et al. (2012) found variability of up to 30% in  $\text{H}\alpha$  emission among a large sample of M0–M9 dwarfs in the field on timescales of minutes to weeks. Thus, the calibration of  $T_{\text{eff}}$  suppression and  $R$  inflation to  $\text{H}\alpha$  emission requires large statistical samples and/or calibration objects with highly accurate measurements in order to identify robust mean relations. Fortunately for this paper, which is concerned with the most highly active young objects which may experience the most significant  $T_{\text{eff}}$  suppression and  $R$  inflation, stronger  $\text{H}\alpha$  emitters also tend to be less time-variable, with the typical  $\text{H}\alpha$  variability being less than 10% for the strongest  $\text{H}\alpha$  emitters (Bell et al. 2012).

In Sec. 2 we describe our approach and the data we use to establish the empirical relationships of  $\Delta T_{\text{eff}}$  and  $\Delta R$  vs.  $L_{\text{H}\alpha}/L_{\text{bol}}$ . In Sec. 3 we present the resulting relations and apply them to 2M0535–05 as a test case, finding that the position of the chromospherically active primary BD in the H-R diagram can be fully explained as an offset from its theoretically expected position, due to the effects of activity on its  $R$  and  $T_{\text{eff}}$  (Fig. 1). In Sec. 4 we discuss the broader application of these relations to other low-mass objects, and their possible ramifications for the inferred IMFs of young clusters. We conclude with a summary in Sec. 5.

## 2. Methods and Data Used

Our aim is to empirically determine a relationship between the temperature suppression (as compared to evolutionary models) and the level of activity as measured from  $\text{H}\alpha$ . We adopt a simple linear form for this relationship:

$$\Delta T_{\text{eff}}/T_{\text{eff}} = m_T \times (\log L_{\text{H}\alpha}/L_{\text{bol}} + 4) + b_T \quad (1)$$

where  $\Delta T_{\text{eff}}/T_{\text{eff}}$  is the fractional temperature offset (observed minus model),  $L_{\text{H}\alpha}/L_{\text{bol}}$  is the ratio of luminosity in the  $\text{H}\alpha$  line to the bolometric luminosity,  $m_T$  and  $b_T$  are linear coefficients, and the offset of +4 is for convenience given the typical value of  $\log L_{\text{H}\alpha}/L_{\text{bol}} \approx -4$  for our study sample (see §3). We determine a similar relationship for the fractional radius inflation:

$$\Delta R/R = m_R \times (\log L_{\text{H}\alpha}/L_{\text{bol}} + 4) + b_R. \quad (2)$$

In the following analysis, we use two different samples and approaches to determine the linear coefficients of Eqs. 1 and 2. In the first approach we use a large sample of stars without direct mass, radius, or  $T_{\text{eff}}$  measurements but with direct distances, spectral types, and reliable  $\text{H}\alpha$  measurements. The second approach uses the much smaller sample of stars in EBs that have directly measured masses, radii, and reliable  $T_{\text{eff}}$ , but for which we must use X-ray flux as a proxy for  $\text{H}\alpha$ .

### 2.1. Nearby M Dwarfs with $\text{H}\alpha$ Emission

We first consider the large set of nearby field M dwarfs with well measured spectral types and  $\text{H}\alpha$  equivalent widths (EWs) from the Palomar/Michigan State University catalog (PMSU; Reid et al. 1995;

Hawley et al. 1996). In particular, following Morales et al. (2008), we restrict ourselves to the sample of 746 stars with distances determined directly from trigonometric parallaxes. These distances allow  $L_{\text{bol}}$  to be calculated from the observed 2MASS  $K_S$  magnitudes together with  $K$ -band bolometric corrections from Bessell et al. (1998). The catalog reported spectral types are transformed to  $T_{\text{eff}}$  according to Leggett et al. (1996) and Bessell (1991). From these  $T_{\text{eff}}$  and  $L_{\text{bol}}$  (Morales et al. 2008, their Tables 1 and 2) we also calculate the stellar radii,  $R$ , according to the usual Stefan-Boltzmann relation. In order to isolate a consistent sample of main-sequence stars as representative as possible of Galactic disk population stars, we removed all stars identified by Morales et al. (2008) as being unresolved binaries, members of young moving groups, part of the old halo population, or evolved subdwarfs. The sample of 746 nearby stars with trigonometric distances is already dominated by field-age disk stars, so these cuts cause only 54 stars to be removed from the sample. We further restricted the sample to those with  $M < 1 M_{\odot}$ , leaving 669 stars in our sample. Finally, we use the solar-metallicity isochrone of Baraffe et al. (1998) with mixing-length  $\alpha=1.0$  to interpolate the predicted stellar masses ( $M$ ),  $T_{\text{eff}}$ , and  $R$  as functions of  $L_{\text{bol}}$ . Our results below do not change significantly for adopted isochrone ages in the range 1–5 Gyr, typical of field star ages for the Galactic disk population, so we adopt the isochrone at 3 Gyr throughout for simplicity.

Fig. 2 shows the estimated  $T_{\text{eff}}$  and  $R$  of the PMSU sample stars as a function of  $M$ . Strongly chromospherically active stars—defined here as those with  $\text{H}\alpha$  in emission—show a clear displacement to lower  $T_{\text{eff}}$  relative to both the theoretical isochrone and to the non-active stars, whereas non-active stars more closely track the isochrone. The  $\text{H}\alpha$  active stars also show a displacement to larger  $R$  relative to both the theoretical isochrone and to the non-active stars. The mean offset of the  $\text{H}\alpha$  active stars relative to the isochrone (solid curve) is  $10.0\sigma$  for  $R$  and  $-11.1\sigma$  for  $T_{\text{eff}}$ , where  $\sigma$  is the standard deviation of the mean (i.e.,  $\text{r.m.s.}/\sqrt{N}$ ). The mean offset relative to the non-active stars (dashed curve) is  $6.8\sigma$  for  $R$  and  $-7.5\sigma$  for  $T_{\text{eff}}$ . The non-active stars themselves show a mild displacement to lower  $T_{\text{eff}}$  and larger  $R$  relative to the theoretical isochrone. We note that at least some of the “non-active” stars in the sample may in fact possess mild chromospheric activity. Mildly active M-type stars can exhibit  $\text{H}\alpha$  in *absorption* (e.g. Walkowicz & Hawley 2009; West et al. 2011) and thus would not be identified as strongly active according to our  $\text{H}\alpha$  emission criterion but could still manifest mild activity-related effects. Alternatively, these offsets for the non-active stars may simply indicate mild systematics in the transformation from the observed  $K$ -band magnitudes into masses and radii via bolometric corrections; indeed, the polynomial fits to the non-active stars closely parallel the theoretical isochrone (except at the highest masses; see also Sec. 3.1). In what follows we conservatively measure the  $T_{\text{eff}}$  and  $R$  offsets of the  $\text{H}\alpha$  active stars relative to the non-active stars, effectively using the latter to calibrate the derived stellar masses and radii to the theoretical isochrone. For reference, the polynomial fits with which we describe the non-active stars (dashed curves in Fig. 2) are:  $R/R_{\odot} = \sum_{i=0}^4 r_i (M/M_{\odot})^i$  and  $T_{\text{eff}}/\text{K} = \sum_{i=0}^4 t_i (M/M_{\odot})^i$ , with  $r_i = \{1.3836, -10.9203, 37.7554, -52.3712, 26.8055\}$  and  $t_i = \{-1384.1, 41857.5, -136147, 192515, -96288.4\}$ , applicable for  $M < 0.8 M_{\odot}$ .

Fig. 3(a) shows the offsets in estimated  $T_{\text{eff}}$  and  $R$  for the  $\text{H}\alpha$  active sample stars as a function of the observed  $\text{EW}(\text{H}\alpha)$ . We fit a simple least-squares linear relation to each (dashed lines), yielding the following:

$$\Delta R/R [\%] = (1.4 \pm 0.8) \times \text{EW}(\text{H}\alpha) [\text{\AA}] + (6.1 \pm 3.2)$$

$$\Delta T_{\text{eff}}/T_{\text{eff}} [\%] = (-0.6 \pm 0.3) \times \text{EW}(\text{H}\alpha) [\text{\AA}] + (-3.0 \pm 1.3).$$

For example, for  $\text{EW}(\text{H}\alpha)=4\text{\AA}$ , the relation predicts a  $T_{\text{eff}}$  suppression of  $\approx 5\%$  and a radius inflation of  $\approx 11\%$ . There is substantial scatter in the data, nonetheless a Kendall’s  $\tau$  correlation test gives a null-hypothesis probability of only 0.9% and 0.7% that the quantities are not correlated in  $\Delta R$  and in  $\Delta T_{\text{eff}}$ , respectively, indicating that the correlations are statistically significant at  $>99\%$  confidence. For comparison, a linear fit

to the  $T_{\text{eff}}$  and  $R$  offsets calculated relative to the theoretical isochrone is shown as a solid line. The linear fit coefficients are nearly identical to those above, except of course for a larger mean offset in both quantities.

To calculate the  $\text{H}\alpha$  luminosity,  $L_{\text{H}\alpha}$ , from the  $\text{EW}(\text{H}\alpha)$  measurements for Equations 1–2, we determined scaling factors from a set of stellar atmosphere models for  $T_{\text{eff}}$  ranging from 3000 to 5000 K in steps of 100 K and  $\log g = 4.0$ . We use the STARDUSTY1999 model spectra, which are based on the NextGen models updated with new  $\text{H}_2\text{O}$  and  $\text{TiO}$  opacities (Allard et al. 2000). We obtain the continuum flux around the  $\text{H}\alpha$  line (6500–6600 Å) for each  $T_{\text{eff}}$ , and we fit the flux– $T_{\text{eff}}$  relation with a third-order polynomial. The measured  $\text{EW}(\text{H}\alpha)$  is then multiplied by the  $\text{H}\alpha$  continuum flux from this relation, and multiplied by the surface area of the star using the measured  $R$  calculated as described above, thus giving the total  $L_{\text{H}\alpha}$ . Fig. 3(b) shows the same data as in Fig. 3(a), but now with  $\text{EW}(\text{H}\alpha)$  converted to  $L_{\text{H}\alpha}/L_{\text{bol}}$ . The resulting relations between the  $T_{\text{eff}}$  and  $R$  offsets vs.  $L_{\text{H}\alpha}/L_{\text{bol}}$  are discussed in Sec. 3.

## 2.2. Low-mass Eclipsing Binary Stars with X-ray Emission

In the second approach, we use the small set of low-mass EBs with accurately measured  $M$ ,  $R$ ,  $T_{\text{eff}}$ , and X-ray luminosities ( $L_X$ ) from López-Morales (2007).<sup>1</sup> The sample includes 11 individual stars in 7 EB systems spanning the range  $T_{\text{eff}}=3125\text{--}5300$  K and  $M=0.21\text{--}0.96 M_{\odot}$ .

We begin with the correlation of  $\Delta R$  vs.  $L_X/L_{\text{bol}}$  already demonstrated in that work, which we rederived (Fig. 4(a)) using the fundamental stellar data compiled in López-Morales (2007) and the same 3 Gyr isochrone of Baraffe et al. (1998) as above. López-Morales (2007) did not discuss the complementary correlation with  $\Delta T_{\text{eff}}$ , but this information is also contained in the EB data, so in Fig. 4(a) we also derive the relationship  $\Delta T_{\text{eff}}$  vs.  $L_X/L_{\text{bol}}$ , again using the data compiled in López-Morales (2007) and the 3 Gyr isochrone of Baraffe et al. (1998). Linear fits are shown for both relations:

$$\Delta R/R [\%] = (15.5 \pm 2.9) \times \log L_X/L_{\text{bol}} + (57 \pm 9)$$

$$\Delta T_{\text{eff}}/T_{\text{eff}} [\%] = (-6.2 \pm 3.2) \times \log L_X/L_{\text{bol}} + (-23 \pm 10).$$

A Kendall’s  $\tau$  correlation test gives a null-hypothesis probability of 0.2% for the correlation with  $\Delta R$ , indicating a significant correlation at 99.8% confidence (see also López-Morales 2007). The correlation with  $\Delta T_{\text{eff}}$  is not as strong, but is nonetheless modestly significant at 94% confidence according to the Kendall’s  $\tau$  test. Interestingly, the  $\Delta R$  and  $\Delta T_{\text{eff}}$  relations, which for the EB sample are measured independently, very nearly offset one another in terms of their effect on  $L_{\text{bol}}$ . For example, at  $\log L_X/L_{\text{bol}} = -3$ , the relations give  $\Delta R \approx 11\%$  and  $\Delta T_{\text{eff}} \approx -5\%$ , implying  $\Delta L_{\text{bol}} \approx 1\%$ . Thus  $L_{\text{bol}}$  is an approximately conserved quantity.

To convert the observed  $L_X/L_{\text{bol}}$  into  $L_{\text{H}\alpha}/L_{\text{bol}}$  for use in Equations 1–2, we use published activity data for two different samples having both X-ray and  $\text{H}\alpha$  emission measurements (see Fig. 5): low-mass stars in young associations (Scholz et al. 2007) and active M dwarfs in the field (Delfosse et al. 1998). Fig. 5 demonstrates that there is a robust correlation between these two quantities over a wide range of activity levels, albeit with considerable scatter. A linear least-squares fit to this correlation is overplotted as solid and dashed line for the first and second sample, respectively. The activity data for M-type field dwarfs published by Reiners & Basri (2007) shows a similar trend (circles in Fig. 5). We note that these correlations can

---

<sup>1</sup>We use the “case 1”  $L_X$  values from López-Morales (2007). The results do not change significantly if we adopt the “case 2” or “case 3”  $L_X$  values instead.

be extended to lower activity levels, as they are consistent with the simultaneous activity data for BDs published by Berger et al. (2010, their Table 5). For the young low-mass stars sample, the fit is:

$$\log(L_X/L_{\text{bol}}) = (1.5 \pm 0.7) \times \log L_{\text{H}\alpha}/L_{\text{bol}} + (3.0 \pm 2.4).$$

For the field M dwarfs and BDs, the fit is:

$$\log(L_X/L_{\text{bol}}) = (1.1 \pm 0.3) \times \log L_{\text{H}\alpha}/L_{\text{bol}} + (1.0 \pm 1.1).$$

For our analysis we have chosen to use the second relation because it better reflects the range of X-ray activity levels observed in the López-Morales (2007) sample of low-mass EBs (see Fig. 4(a)). This is also a more conservative choice, in that it associates a lower  $L_X/L_{\text{bol}}$  for a given  $L_{\text{H}\alpha}/L_{\text{bol}}$ , and therefore will predict smaller absolute  $\Delta T_{\text{eff}}$  and  $\Delta R$  offsets for a given observed  $L_{\text{H}\alpha}/L_{\text{bol}}$ .

Fig. 4(b) shows the same data as in Fig. 4(a), but now with  $L_X/L_{\text{bol}}$  converted to  $L_{\text{H}\alpha}/L_{\text{bol}}$ . The resulting relations between the  $T_{\text{eff}}$  and  $R$  offsets vs.  $L_{\text{H}\alpha}/L_{\text{bol}}$  are discussed in Sec. 3.

### 3. Results

#### 3.1. Empirical Relations Linking $T_{\text{eff}}$ Suppression and Radius Inflation to $\text{H}\alpha$ Emission

We have determined empirical relationships linking the degree of temperature suppression,  $\Delta T_{\text{eff}}/T_{\text{eff}}$ , and radius inflation,  $\Delta R/R$ , to the fractional  $\text{H}\alpha$  luminosity,  $L_{\text{H}\alpha}/L_{\text{bol}}$ , using two independent samples and methods (see Figs. 3(b) and 4(b)). The fit coefficients from Eqs. 1–2 for the two samples are summarized in Table 1. The fit coefficients are defined such that the left-hand side (LHS) of Eqs. 1–2 are in percent units.

The  $\Delta T_{\text{eff}}$  and  $\Delta R$  fit coefficients in Table 1 are consistent to within 1–2 $\sigma$  between the two samples, although the formal uncertainties on the fit parameters are large for the field M-dwarf sample. This likely reflects the large scatter in the  $\text{H}\alpha$  measurements for that sample, perhaps stemming from intrinsic stellar variability. In addition, for the field M-dwarf sample the determination of  $L_{\text{H}\alpha}/L_{\text{bol}}$  involved several calculated quantities (i.e.,  $R$ ,  $L_{\text{bol}}$ ) whereas for the EB sample these stellar parameters are measured directly and accurately. Indeed, for the field M-dwarfs the statistical significance of the  $\Delta T_{\text{eff}}$  and  $\Delta R$  correlations was stronger *before* we converted the directly measured  $\text{EW}(\text{H}\alpha)$  to  $L_{\text{H}\alpha}/L_{\text{bol}}$ . Even so, both the  $\Delta T_{\text{eff}}$  and the  $\Delta R$  relations for both samples are confirmed to be significantly correlated with  $L_{\text{H}\alpha}/L_{\text{bol}}$  according to a Kendall’s  $\tau$  test (Table 1). Being a non-parametric rank-correlation test, Kendall’s  $\tau$  does not depend on the assumed functional form of the relationship, and thus robustly indicates the presence of a correlation even if the significance of the assumed functional parameters is modest.

For our final best-fit relation, we calculated the weighted average of the fit parameters for the two samples. The resulting best-fit coefficients for Eqs. 1 and 2 are also listed in Table 1, and the corresponding final fits shown in Figure 6. As is evident in Fig. 6, the r.m.s. scatter of the data about the mean relations is large (4.2% and 9.2% for  $\Delta T_{\text{eff}}$  and  $\Delta R$ , respectively), driven primarily by the scatter in the field M-dwarf data (see Sec. 2.1). Nonetheless, the statistical significance of the final combined relations is strong (Table 1).

The input samples used to determine these relations include low-mass stars with  $0.2 < M < 1 M_{\odot}$ . There is no evidence that the  $T_{\text{eff}}$  suppression and  $R$  inflation effects change qualitatively at lower masses (see Fig. 2), and we are able to validate them successfully at BD masses (see below). However, the relations appear to diverge at masses  $\gtrsim 0.8 M_{\odot}$  (see Fig. 2) and so we caution against their use at such high masses. Given the range of  $L_{\text{H}\alpha}/L_{\text{bol}}$  spanned by the input data samples, these relations are applicable for  $-4.6 \lesssim$

Table 1. Fit parameters for Equations 1 and 2

	$m$	$b$	$\tau$ conf. <sup>a</sup>
Field M-dwarfs <sup>b</sup>			
$\Delta T_{\text{eff}}$	$-3.12 \pm 3.15$	$-5.1 \pm 0.7$	92.9%
$\Delta R$	$8.00 \pm 7.63$	$11.2 \pm 1.6$	91.2%
Eclipsing Binaries <sup>c</sup>			
$\Delta T_{\text{eff}}$	$-6.64 \pm 3.47$	$-3.0 \pm 1.0$	94.3%
$\Delta R$	$16.64 \pm 3.15$	$6.6 \pm 0.6$	99.8%
Averaged Final Relation <sup>d</sup>			
$\Delta T_{\text{eff}}$	$-4.71 \pm 2.33$	$-4.4 \pm 0.6$	96.0%
$\Delta R$	$15.37 \pm 2.91$	$7.1 \pm 0.6$	98.6%

<sup>a</sup>Statistical confidence of correlation from Kendall’s  $\tau$  test.

<sup>b</sup>See Fig. 3(b).

<sup>c</sup>See Fig. 4(b).

<sup>d</sup>See Fig. 6.

Note. — The fit parameters are defined such that the LHS of Equations 1–2 are in percent units.

$\log L_{\text{H}\alpha}/L_{\text{bol}} \lesssim -3.4$  (see Fig. 6), the upper limit corresponding approximately to the empirical “saturation” level of  $\log L_{\text{H}\alpha}/L_{\text{bol}} \approx -3.3$  observed in low-mass stars and BDs (e.g. Barrado y Navascués & Martín 2003). Therefore the relations likely cannot be extrapolated to  $\log L_{\text{H}\alpha}/L_{\text{bol}} > -3.3$ . Note also that for  $\log L_{\text{H}\alpha}/L_{\text{bol}} \lesssim -4.6$ , Eqs. 1–2 give *positive*  $\Delta T_{\text{eff}}$  and *negative*  $\Delta R$ , which is likely not physical. More likely the  $\Delta T_{\text{eff}}$  and  $\Delta R$  offsets simply approach zero at very low activity levels, and thus we caution that our relations should not be extrapolated to arbitrarily low  $L_{\text{H}\alpha}$ .

### 3.2. Application to 2M0535–05

2M0535–05 is to date the only known system of BDs with directly and accurately measured masses, radii,  $T_{\text{eff}}$ , and  $L_{\text{H}\alpha}$ , all at a well constrained system age (Stassun et al. 2006, 2007; Gómez Maqueo Chew et al. 2009). 2M0535–05 is therefore an important empirical test case for assessing the efficacy of the activity-based  $\Delta T_{\text{eff}}$  and  $\Delta R$  relations that we have determined above. The known masses of the primary and secondary BDs in 2M0535–05 are  $60 \pm 3$  and  $39 \pm 2$   $M_{\text{Jup}}$ , respectively.

To demonstrate how the *apparent* masses of the 2M0535–05 primary and secondary BDs are altered by our empirical relations, we calculate how the observed positions of the two BDs in the H-R diagram are altered by adjusting the observed  $T_{\text{eff}}$  and  $R$  using Eqs. 1–2 and Table 1. In effect, we are using our empirical relations to show how the 2M0535–05 system would appear in the H-R diagram were the system completely inactive. The spectral type of  $M6.5 \pm 0.5$  for 2M0535–05 determined by Stassun et al. (2006) from high-resolution  $H$ -band spectroscopy implies an average  $T_{\text{eff}} = 2688 \pm 55$  K, based on the near-infrared spectral-type– $T_{\text{eff}}$  relation of Slesnick et al. (2004). Weighting this average  $T_{\text{eff}}$  by the  $H$ -band primary-to-secondary flux ratio of 1.6:1 found by Stassun et al. (2007) and using the accurately determined  $T_{\text{eff}}$  ratio of  $T_1/T_2 = 0.952 \pm 0.004$  (Gómez Maqueo Chew et al. 2009) then gives  $T_{\text{eff}} = 2640 \pm 60$  and  $T_{\text{eff}} = 2770 \pm 60$  K for the primary and secondary components, respectively. These individual  $T_{\text{eff}}$  together with the accurately measured individual radii (Stassun et al. 2007; Gómez Maqueo Chew et al. 2009) then give the individual  $L_{\text{bol}}$ . These observed  $T_{\text{eff}}$  and  $L_{\text{bol}}$  for the primary and secondary components are represented in Fig. 1 as blue symbols, from which one would infer masses (using the Baraffe et al. evolutionary models) of  $\approx 27$  and  $\approx 40$   $M_{\text{Jup}}$ , respectively, based on the observed  $T_{\text{eff}}$ . That is, the inactive secondary is inferred to have approximately its true mass, but the active primary appears to have a mass that is a factor of 2 lower than its true mass, and moreover the primary appears to be much younger than its (presumably coeval) companion.

We use the  $L_{\text{H}\alpha}/L_{\text{bol}}$  measurements of Reiners et al. (2007), who found  $\log L_{\text{H}\alpha}/L_{\text{bol}} = -3.47$  for the active primary and  $\log L_{\text{H}\alpha}/L_{\text{bol}} < -4.30$  (upper limit) for the inactive secondary. From Eqs. 1 and 2, we find that the primary has been displaced from its inactive  $T_{\text{eff}}$  by an amount  $\Delta T_{\text{eff}} = -6.9 \pm 1.4\%$ , and displaced from its inactive  $R$  by an amount  $\Delta R = 15.2 \pm 1.7\%$ . For the secondary, the resulting  $\Delta T_{\text{eff}}$  is at most  $-3.0 \pm 0.9\%$ , and  $\Delta R$  is at most  $2.5 \pm 1.1\%$ . For both BDs the  $\Delta T_{\text{eff}}$  and  $\Delta R$  displacements nearly cancel such that  $L_{\text{bol}}$  is preserved to within 1–3%.

As shown in Fig. 1, shifting the H-R diagram position of the primary BD according to its calculated  $\Delta T_{\text{eff}}$  and  $\Delta R$  shows that, if it were inactive, it would be in remarkably good agreement with the theoretically expected position for its known mass. The observed  $L_{\text{H}\alpha}/L_{\text{bol}}$  of the active primary is near the “saturation” limit and therefore near the upper limit of observed activity levels in young low-mass objects, for which the  $\text{H}\alpha$  emission is found to be mostly non-variable (e.g. Bell et al. 2012). Thus we do not expect a large contribution to the uncertainty of the active primary in Fig. 1 due to  $\text{H}\alpha$  variability. We do not shift the position of the secondary as its  $L_{\text{H}\alpha}$  is an upper limit only.



## 4. Discussion

### 4.1. $H\alpha$ , magnetic activity, and cooled/inflated stars

In developing these empirical relationships, we posit a correlation between chromospheric activity, radius inflation, and  $T_{\text{eff}}$  suppression, where activity is implicitly tied to magnetic fields. Chabrier et al. (2007) and MacDonald & Mullan (2009) have suggested that a sufficiently strong field could suppress convection, inhibit heat transfer, and thus inflate (and cool) the stellar surface. Since such a field would also likely result in chromospheric activity, one might therefore expect the correlations that we have derived. However, there are two significant outstanding questions in creating the above link: (1) Is the relation between  $H\alpha$  emission, field strength, and radius inflation /  $T_{\text{eff}}$  suppression monotonic? (2) Are the magnetic fields in fully convective objects strong enough to account for the radius inflation and  $T_{\text{eff}}$  suppression?

First, it remains unclear how well  $H\alpha$  emission correlates with the strength of the magnetic field. Reiners & Basri (2007) have attempted to relate field strength and  $L_{H\alpha}/L_{\text{bol}}$  using the FeH line. They find a correlation between the two, but with different power law scalings for different spectral types. Whether this is an age or mass effect remains uncertain. While this correlation is encouraging for the empirical relations we provide here, Reiners & Basri (2007) use slowly rotating field stars, whose magnetic properties may differ from the most active (younger) objects in which we are interested. As noted previously,  $H\alpha$  emission is also variable, though the most active objects typically have the lowest variability (Bell et al. 2012). Concurrent multi-wavelength monitoring of multiple chromospheric tracers including radio and X-ray, show that the individual tracers do not always vary on the same timescales (Berger 2006; Berger et al. 2008). Thus it is unclear that any individual wavelength range is representative of the total energy contained in the field. Despite these different trends in variability, that  $L_X$  also correlates with  $T_{\text{eff}}$  suppression and radius inflation (see Fig. 4(a)) corroborates our use of chromospheric activity to account for the displacement of objects from model isochrones (see also, e.g., Morales et al. 2008, and references therein).

The second concern, whether or not magnetic fields are sufficiently powerful to inflate the stars and suppress their surface temperatures, is currently impossible to address without appealing to models. Browning (2008) has shown in global numerical models that fully convective stars can host large Kilogauss strength fields, but these alone are too weak to produce the observed radius inflation and  $T_{\text{eff}}$  suppression in 2M0535–05 (MacDonald & Mullan 2009). Chabrier et al. (2007) also suggest that fully convective objects should be less affected by the same convective inefficiencies invoked to explain radius discrepancies at higher masses. It is possible that a combination of rotation and magnetic activity contribute to both inflation/suppression and  $H\alpha$  emission in such a way as to produce our empirical relation without a causal correspondence between  $H\alpha$  and the magnetic field.

An alternative explanation for stars with  $T_{\text{eff}}$  deficits is a spot covered surface (e.g. Lacy 1977). For the case of 2M0535–05, Mohanty et al. (2010) have argued that a model for the active primary with 70% (axisymmetric) spot coverage could explain the peculiar mass-temperature relationship in that system. Since spot coverage is also controlled by magnetic fields, a correlation with  $H\alpha$  might still exist. It remains unclear how to interpret spot coverage of greater than 50%; perhaps the analogy with solar type spots breaks down in such extreme systems. Indeed, Mohanty & Stassun (2012) have now shown from a spectral fine-analysis of the 2M0535–05 system, observed at high resolving power during both primary and secondary eclipses, that such a large-spot scenario is strongly disfavored as an explanation for the  $T_{\text{eff}}$  suppression of the primary BD in 2M0535–05. Thus, while the  $T_{\text{eff}}$  suppression mechanism produces a clear correlation with chromospheric  $H\alpha$  activity as we have shown here, it evidently does not in all cases effect this correlation directly through surface spots.

#### 4.2. Impact on estimates of object masses

The vast majority of masses for stars and BDs in young clusters can only be determined by comparison with theoretical evolutionary tracks in H-R diagrams, using either luminosity or  $T_{\text{eff}}$  or both (e.g. Kenyon & Hartmann 1995; Hillenbrand 1997; Luhman et al. 1998; Moraux et al. 2007; Scholz et al. 2012). While direct mass measurements are available for calibration of these models at higher masses ( $M \gtrsim 0.3 M_{\odot}$ ; e.g., Hillenbrand & White 2004), at the lowest stellar masses and into the substellar regime these models are essentially untested. Therefore, if there is indeed a relation between magnetic activity and  $R$  inflation /  $T_{\text{eff}}$  suppression, this will also affect estimates of stellar and substellar masses derived from  $T_{\text{eff}}$ , especially at young ages when activity levels are high. In the following, we examine two ways of estimating masses that are commonly used in the literature and investigate the impact of magnetic activity on the derived masses.

First we use  $T_{\text{eff}}$  to estimate masses from model isochrones at 1 Myr. At each model mass, we consider a range of activity levels and apply offsets to the model  $T_{\text{eff}}$  based on our Eq. 1 (using “averaged final” coefficients from Table 1). We then use these suppressed  $T_{\text{eff}}$  values to estimate the masses that would be inferred from the isochrone. The resulting curves are shown in the upper panel of Fig. 7. (Note that for  $\log L_{\text{H}\alpha}/L_{\text{bol}} = -4.7$  the offset with Eq. 1 becomes zero.) We consider masses of 0.02–0.60  $M_{\odot}$  (i.e.,  $T_{\text{eff}} = 2500\text{--}3500$  K), for which we use a combination of BCAH (Baraffe et al. 1998) and Dusty (Allard et al. 2001) isochrones. (Using BCAH models at masses  $\geq 0.1 M_{\odot}$  and Dusty models at lower masses, we fit a third order polynomial to mass as a function of  $T_{\text{eff}}$ .)

As expected, this procedure leads to a systematic *underestimation* of the masses. At high levels of activity, the effect can be substantial. For  $\log L_{\text{H}\alpha}/L_{\text{bol}} = -3.3$ , which corresponds to the saturation limit in young low-mass stars (Barrado y Navascués & Martín 2003) and the upper limit of the observed H $\alpha$  activity in young associations (Scholz et al. 2007), the mass estimates are a factor of  $\sim 2$  lower than for objects with low levels of magnetic activity ( $\log L_{\text{H}\alpha}/L_{\text{bol}} < -4.5$ ). In Fig. 7 we overplot the datapoint for the primary component of the eclipsing BD 2M0535–05. As discussed above, its mass would be estimated to be 0.03  $M_{\odot}$ , whereas its true mass is about twice as high. We note that because the mass- $T_{\text{eff}}$  relationship is less steep at older ages, the underestimation of mass is less severe at older ages ( $\gtrsim 100$  Myr).

In the second test case, we use  $L_{\text{bol}}$  derived from  $K$ -band absolute magnitudes to derive masses. In this case the influence of magnetic activity is introduced by the  $T_{\text{eff}}$  dependence of the bolometric correction, since the bolometric luminosities are (as outlined above) practically not affected. We consider the same range of masses as in the first case, and we compute spectral types from the suppressed values of  $T_{\text{eff}}$  using the relation of Luhman (2003, fitted linearly). We then computed  $K$ -band bolometric corrections from Slesnick et al. (2004) from the spectral types, and we combine these with the model  $K$ -band absolute magnitudes to find  $L_{\text{bol}}$  (we used a linear fit of model  $M_K$  as a function of  $T_{\text{eff}}$ ). Finally, we estimated masses from the model isochrone and  $L_{\text{bol}}$ , and the result is shown in the lower panel of Fig. 7.

This second method still leads to an underestimate of the masses, but the effect is much smaller than when directly estimating masses from  $T_{\text{eff}}$ . The curves are almost flat, i.e. the estimated masses depend insignificantly on the level of magnetic activity. The change of the bolometric corrections with increasing magnetic activity is quite small (at most 10%), resulting in relatively minor changes of a few percent in the mass estimate. With this method, the mass for the primary component of the eclipsing BD 2M0535–05 would be 0.054  $M_{\odot}$  and thus only marginally smaller than the true value.

These effects are systematic biases in estimated masses due to  $T_{\text{eff}}$  suppression, so this will always be significant for statistical studies of populations (e.g., in young clusters). For individual objects, this bias

may be somewhat lower than the uncertainty in  $T_{\text{eff}}$  due simply to our limited ability to accurately model spectra of 2500–3500 K objects. For example, the best benchmark objects currently available over the 2500–3000 K range—very low-mass stars and BDs with dynamical mass measurements—show that model atmospheres likely harbor large systematic errors ( $\approx 250$  K; Dupuy et al. 2010). This uncertainty corresponds to a fractional error in  $T_{\text{eff}}$  of  $\approx 8\%$ – $10\%$ , which is somewhat larger than the typical offset we find due to  $T_{\text{eff}}$  suppression.

An important application of  $T_{\text{eff}}$ -based mass estimates is the determination of mass functions (MFs) for young clusters. Typical early to mid M-type dwarfs with ages from 10 to 100 Myr exhibit  $\text{H}\alpha$  emission in the range  $\log L_{\text{H}\alpha}/L_{\text{bol}} = -4.2$  to  $-3.3$  (Barrado y Navascués & Martín 2003; Scholz et al. 2007). For BDs at the same ages the available data are sparse but indicate an upper limit around  $-3.7$  (Barrado y Navascués & Martín 2003). Thus, the upper panel of Fig. 7 implies that objects inferred to be BDs from  $T_{\text{eff}}$ -based (or spectral type based) mass estimates could actually be low-mass stars since masses will be underestimated by up to a factor of 2.

We further evaluated the impact of this effect on measurements of the slope of the mass function,  $\alpha$  (in  $dN/dM \propto M^{-\alpha}$ ). For this purpose, we assume a measured slope of  $\alpha = 0.6$ , which is consistent with a number of studies in very young clusters (see Scholz et al. 2012, submitted, and references therein), calculate the mass function based on that slope for  $M < 0.6 M_{\odot}$ , correct the masses for a given level of  $\text{H}\alpha$  emission using the results given above, and re-determine the slope  $\alpha$ . If magnetic activity and thus the level of  $\text{H}\alpha$  emission is constant across the low-mass regime,  $\alpha$  is practically unchanged, because all masses will be underestimated by about the same factor. Based on the available measurements, however, it seems more realistic to assume that BDs have on average a lower level of activity than low-mass stars (Barrado y Navascués & Martín 2003). If we start with  $\log L_{\text{H}\alpha}/L_{\text{bol}} = -4.0$  for BDs and  $-3.5$  for low-mass stars, the masses have to be corrected by factors of 1.3–1.7 for BDs, and by 2.2–2.5 for low-mass stars. As a result, the slope changes from  $\alpha = 0.6$  to  $\alpha = 0.5$ . A more extreme mass dependence of the activity level will enhance this effect. In general, we expect that  $\alpha$  will be underestimated by  $\gtrsim 0.1$ , if the masses are estimated from  $T_{\text{eff}}$  and activity is not taken into account. In addition, the peak of the mass function could be underestimated by up to a factor of 2. For a more quantitative assessment of these effects a larger sample of  $\text{H}\alpha$  measurements for young stars and BDs is needed.

## 5. Conclusions

In this paper, we have shown that there exists a correlation between the strength of  $\text{H}\alpha$  emission in active M-dwarfs, and the degree to which their temperatures are suppressed and radii inflated compared with inactive objects and theoretical evolutionary models. By applying these relations, we are able to infer the amount by which an active objects’ temperatures have been suppressed, and thereby improve the accuracy of estimates for their masses and radii. We use the brown dwarf eclipsing binary system 2M0535–05 as a benchmark for our model. We expect these relations to be most useful for correcting estimated masses and radii of low-mass stars and brown dwarfs over their active lifetimes (few Gyr; West et al. 2008) and when the ages or distances (and therefore the luminosities) are unknown. We have shown that failing to account for the effects of activity can cause significant errors in estimates of stellar and substellar masses derived from  $T_{\text{eff}}$ , and smaller, but systematically biased errors in temperature and radius.

If these empirical corrections are corroborated by future observations, they will prove valuable not only for individual objects, but also for studies of stellar populations. In the case of individual objects,

reliable stellar properties are invaluable for exoplanetary studies, where exquisite knowledge of the host star is required to infer planet properties. For very young stellar populations, where activity levels are highest, we have shown how underestimated masses can substantially shift the inferred initial mass function. Such a change would necessitate revisions to star formation models and population synthesis models because, e.g., the observed fraction of brown dwarfs and low-mass stars might be substantially altered.

While promising, the correlations we have derived contain significant scatter, and they are currently limited by the lack of a single sample of stars with both  $H\alpha$  and direct radius measurements. A sample of  $H\alpha$  measurements for objects with directly measured radii and temperatures will allow us to better assess our relations and determine if the scatter is intrinsic or if it is caused by the intermediate steps necessary in constructing our relation (e.g., converting  $L_X$  to  $L_{H\alpha}$ ). Despite this limitation, we have chosen to pursue a correlation with  $H\alpha$  emission (rather than X-ray, or radio, for example) because of the relative ease of its measurement even in the substellar regime. In principle, a reliable activity tracer in the near-IR would prove even more useful by making measurements easier for cooler objects. No such tracer has yet been identified (see, e.g., Schmidt et al. 2012), although the He I line at 10830Å may be a possibility (e.g. Dupree et al. 1992).

In order to make progress on understanding how  $T_{\text{eff}}$  suppression and radius inflation relate to chromospheric activity, a larger sample of EBs with precise masses, radii, *and*  $H\alpha$  measurements are needed. Toward this goal, we encourage other researchers to publish  $H\alpha$  measurements for their targets, as this is usually readily available from the spectra used to determine radial velocities. Indeed, a number of low-mass EBs with accurate masses and radii have been published in the last few years (e.g. Vaccaro et al. 2007; Irwin et al. 2009; Morales et al. 2010; Kraus et al. 2011; Helminiak et al. 2011; Helminiak & Konacki 2011; Irwin et al. 2011), potentially increasing by a factor of 2–3 the small sample that we have used from López-Morales (2007). We are currently collecting new  $H\alpha$  measurements for these published EBs that lack resolved  $H\alpha$  measurements in order to improve the empirical relations that we have presented here.

Finally, the relations we have determined already indicate quite clearly that the radius inflation and temperature suppression mechanism operates in such a way that the temperature suppression and radius inflation almost exactly cancel in terms of their effect on the bolometric luminosity. Moreover, the relations between activity,  $T_{\text{eff}}$  suppression, and radius inflation do not appear to manifest any obvious discontinuity across the fully convective transition (see also Stassun et al. 2010); the followup observations we have underway should help to refine this. These are important, fundamental clues to the physical nature of these effects, and should help to constrain theoretical models that are being developed to explain these phenomena (e.g. Chabrier et al. 2007; MacDonald & Mullan 2009).

We thank Beate Stelzer for helpful discussions. K.G.S. acknowledges NSF grants AST-0607773 and AST-1009810. Part of this work was funded by the Science Foundation Ireland through grant no. 10/RFP/AST2780 to A.S. T.J.D. acknowledges support from Hubble Fellowship grant HST-HF-51271.01-A awarded by the Space Telescope Science Institute, which is operated by AURA for NASA, under contract NAS 5-26555.

## REFERENCES

- Allard, F., Hauschildt, P. H., & Schwenke, D. 2000, *ApJ*, 540, 1005
- Allard, F., Hauschildt, P. H., Alexander, D. R., Tamanai, A., & Schweitzer, A. 2001, *ApJ*, 556, 357

- Bell, K. J., Hilton, E. J., Davenport, J. R. A., et al. 2012, *PASP*, 124, 14
- Baraffe, I., Chabrier, G., Allard, F., & Hauschildt, P. H. 1998, *A&A*, 337, 403
- Barrado y Navascués, D., & Martín, E. L. 2003, *AJ*, 126, 2997
- Bell, K. J., Hilton, E. J., Davenport, J. R. A., et al. 2012, *PASP*, 124, 14
- Berger, E., Basri, G., Fleming, T. A., et al. 2010, *ApJ*, 709, 332
- Berger, E., Basri, G., Gizis, J. E., et al. 2008, *ApJ*, 676, 1307
- Berger, E. 2006, *ApJ*, 648, 629
- Bessell, M. S., Castelli, F., & Plez, B. 1998, *A&A*, 333, 231
- Bessell, M. S. 1991, *AJ*, 101, 662
- Browning, M. K. 2008, *ApJ*, 676, 1262
- Burgasser, A. J., Marley, M. S., Ackerman, A. S., et al. 2002, *ApJ*, 571, L151
- Chabrier, G., Gallardo, J., & Baraffe, I. 2007, *A&A*, 472L, 17
- Coughlin, J. L., López-Morales, M., Harrison, T. E., Ule, N., & Hoffman, D. I. 2011, *AJ*, 141, 78
- Da Rio, N., Robberto, M., Hillenbrand, L. A., Henning, T., & Stassun, K. G. 2012, *ApJ*, 748, 14
- Delfosse, X., Forveille, T., Perrier, C., & Mayor, M. 1998, *A&A*, 331, 581
- Dupree, A. K., Sasselov, D. D., & Lester, J. B. 1992, *ApJ*, 387, L85
- Dupuy, T. J., Liu, M. C., Bowler, B. P., et al. 2010, *ApJ*, 721, 1725
- Gómez Maqueo Chew, Y., Stassun, K. G., Prša, A., & Mathieu, R. D. 2009, *ApJ*, 699, 1196 (G09)
- Hawley, S. L., Gizis, J. E., & Reid, I. N. 1996, *AJ*, 112, 2799
- Helminiak, K. G., Konacki, M., Złoczewski, K., et al. 2011, *A&A*, 527, A14
- Helminiak, K. G., & Konacki, M. 2011, *A&A*, 526, A29
- Hillenbrand, L. A. 1997, *AJ*, 113, 1733
- Hillenbrand, L. A., & White, R. J. 2004, *ApJ*, 604, 741
- Irwin, J. M., Quinn, S. N., Berta, Z. K., et al. 2011, *ApJ*, 742, 123
- Irwin, J., Charbonneau, D., Berta, Z. K., et al. 2009, *ApJ*, 701, 1436
- Kenyon, S. J., & Hartmann, L. 1995, *ApJS*, 101, 117
- Kraus, A. L., Tucker, R. A., Thompson, M. I., Craine, E. R., & Hillenbrand, L. A. 2011, *ApJ*, 728, 48
- Lacy, C. H., *ApJ* 1977, 218, 444
- Leggett, S. K., Allard, F., Berriman, G., Dahn, C. C., & Hauschildt, P. H. 1996, *ApJS*, 104, 117

- López-Morales, M. 2007, *ApJ*, 660, 732
- Luhman, K. L., Rieke, G. H., Lada, C. J., & Lada, E. A. 1998, *ApJ*, 508, 347
- Luhman, K. L. 2003, *Brown Dwarfs*, 211, 103
- MacDonald, J. & Mullan, D.J., 2009, *ApJ*, 700, 387
- Mohanty, S., & Stassun, K. G. 2012, *ApJ*, in press
- Mohanty, S., Stassun, K. G., & Doppmann, G. W. 2010, *ApJ*, 722, 1138
- Mohanty, S., Stassun, K. G., & Mathieu, R. D. 2009, *ApJ*, 697, 713
- Morales, J. C., Gallardo, J., Ribas, I., et al. 2010, *ApJ*, 718, 502
- Morales, J. C., Ribas, I., & Jordi, C. 2008, *A&A*, 478, 507
- Moraux, E., Bouvier, J., Stauffer, J. R., Barrado y Navascués, D., & Cuillandre, J.-C. 2007, *A&A*, 471, 499
- Reid, I. N., Hawley, S. L., & Gizis, J. E. 1995, *AJ*, 110, 1838
- Reiners, A., Seifahrt, A., Stassun, K. G., Melo, C., & Mathieu, R. D. 2007, *ApJ*, 671L, 149
- Reiners, A., & Basri, G. 2007, *ApJ*, 656, 1121
- Ribas, I. 2006, *Ap&SS*, 304, 89
- Schmidt, S. J., Kowalski, A. F., Hawley, S. L., Hilton, E. J., Wisniewski, J. P., & Tofflemire, B. M. 2012, *ApJ*, 745, 14
- Scholz, A., Coffey, J., Brandeker, A., & Jayawardhana, R. 2007, *ApJ*, 662, 1254
- Scholz, A., Muzic, K., Geers, V., et al. 2012, *ApJ*, 744, 6
- Slesnick, C. L., Hillenbrand, L. A., & Carpenter, J. M. 2004, *ApJ*, 610, 1045
- Stassun, K. G., Hebb, L., Covey, K., et al. 2010, in *Cool Stars & the Sun XVI*. arXiv:1012.2580
- Stassun, K. G., Hebb, L., López-Morales, M., & Prša, A. 2009, *IAU Symposium*, 258, 161
- Stassun, K. G., Mathieu, R. D., & Valenti, J. A. 2007, *ApJ*, 664, 1154
- Stassun, K. G., Mathieu, R. D., & Valenti, J. A. 2006, *Nature*, 440, 311
- Torres, G., Andersen, J., & Giménez, A. 2010, *A&A Rev.*, 18, 67
- Vaccaro, T. R., Rudkin, M., Kawka, A., et al. 2007, *ApJ*, 661, 1112
- Walkowicz, L. M., & Hawley, S. L. 2009, *AJ*, 137, 3297
- West, A. A., Morgan, D. P., Bochanski, J. J., et al. 2011, *AJ*, 141, 97
- West, A. A., Hawley, S. L., Bochanski, J. J., et al. 2008, *AJ*, 135, 785

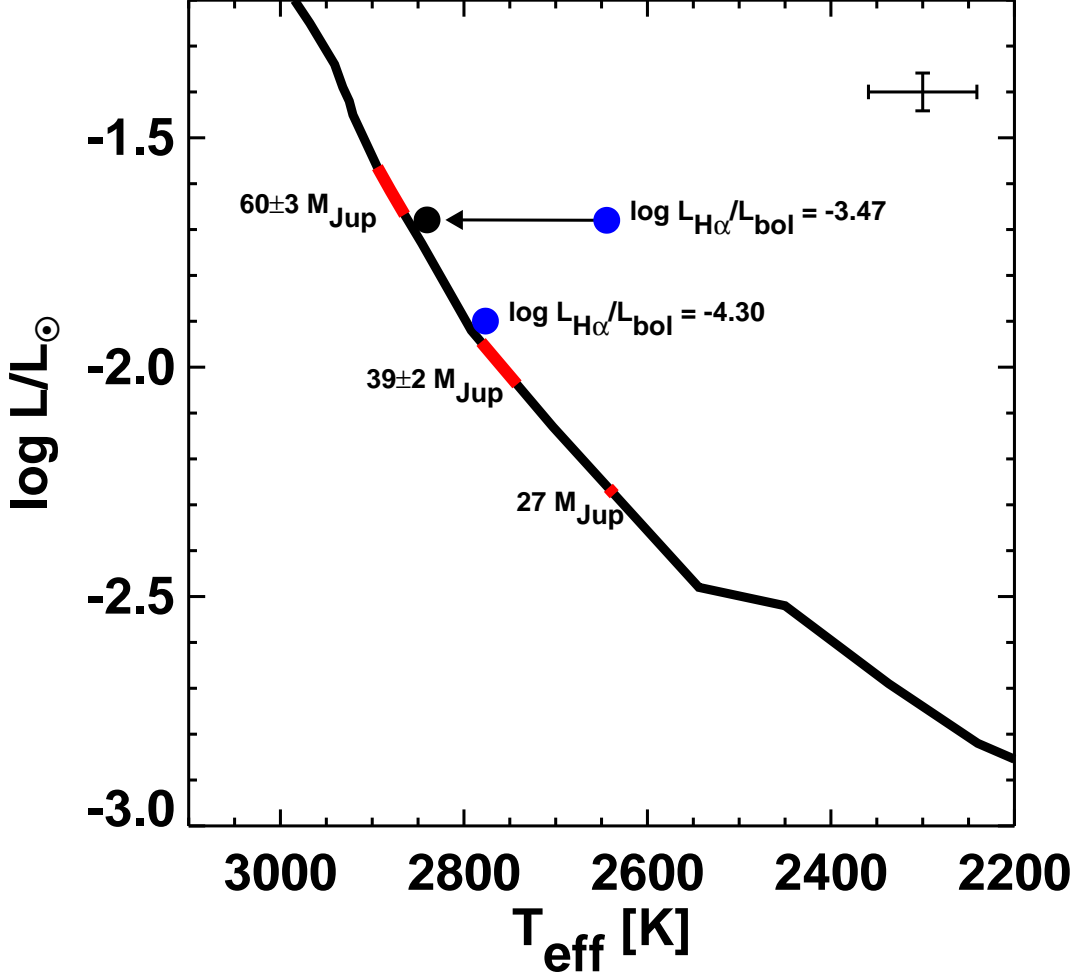


Fig. 1.— Hertzsprung-Russell diagram for the primary and secondary components of the brown-dwarf eclipsing binary 2M0535–05 in the  $\sim 1$ -Myr Orion Nebula Cluster (Stassun et al. 2006, 2007; Gómez Maqueo Chew et al. 2009). The measured  $T_{\text{eff}}$  and  $L_{\text{bol}}$  (the latter calculated from the directly measured  $T_{\text{eff}}$ ’s and radii; see Sec. 3.2) for both brown dwarfs are represented as blue symbols. Measurement uncertainties in  $T_{\text{eff}}$  and  $L_{\text{bol}}$  are represented by the error bars at upper right. The dynamically measured masses of the primary and secondary are  $60 \pm 3$  and  $39 \pm 2$   $M_{\text{Jup}}$ , respectively, represented as red bars on the 1-Myr theoretical isochrone of Baraffe et al. (1998). The measured  $L_{\text{H}\alpha}/L_{\text{bol}}$  for the two components from Reiners et al. (2007) are indicated next to the blue symbols. The inactive secondary appears close to its expected position on the isochrone, whereas the active primary appears far cooler than expected. The primary therefore appears to be much younger than the secondary and to have a mass of only  $\approx 27$   $M_{\text{Jup}}$  based on its observed  $T_{\text{eff}}$ , a factor of 2 lower than its true mass. Shifting the position of the active primary (arrow) using our empirically calibrated  $\text{H}\alpha$ -based relations for  $T_{\text{eff}}$  suppression and radius inflation brings the primary into much closer agreement with its theoretically expected position in the HR diagram (black symbol); this is where the active primary would be if it were not active. This figure is shown in color in the electronic version only.

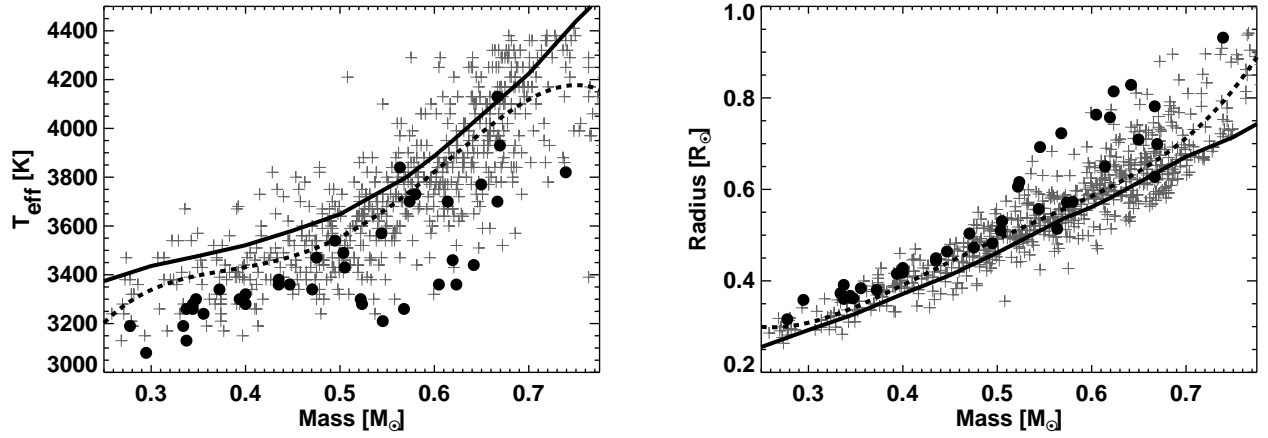


Fig. 2.— Effective Temperature vs. Mass (left) and Radius vs. Mass (right) for M-dwarfs with trigonometric distances and  $H\alpha$  measurements from the PMSU catalog. Active objects (i.e., those with  $H\alpha$  in emission) are represented by filled symbols. For reference, the 3 Gyr theoretical isochrone of Baraffe et al. (1998) is represented in both figures as a solid curve. A polynomial fit to the non-active objects is represented by a dashed curve. The  $H\alpha$ -active dwarfs are found to be significantly displaced to lower  $T_{\text{eff}}$  and larger radii as compared to both the theoretical isochrone and the non-active dwarfs.



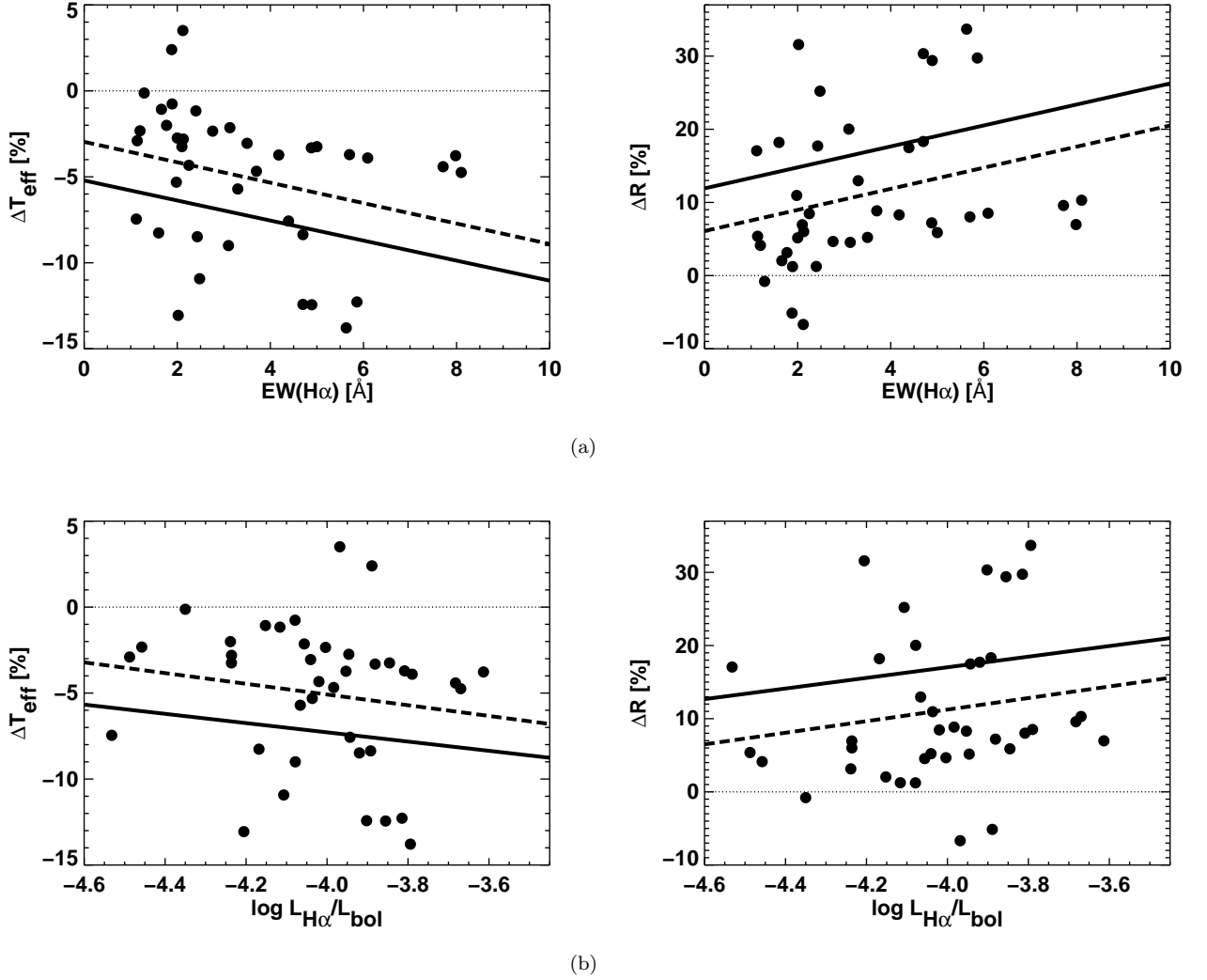


Fig. 3.— Suppression of effective temperatures (left) and inflation of radii (right) as a function of H $\alpha$  emission strength for the H $\alpha$ -active sample from Fig. 2 (filled symbols), measured relative to the non-active stars. In (top), the abscissa is the directly measured H $\alpha$  equivalent width, in (bottom) the H $\alpha$  equivalent widths have been converted to fractional H $\alpha$  luminosity. In all panels, the solid line is a linear fit to the  $T_{\text{eff}}$  and radius differences relative to the theoretical isochrone (solid curves in Fig. 2); the dashed line is a linear fit to the  $T_{\text{eff}}$  and radius differences relative to the non-active stars (dashed curves in Fig. 2). For our analysis we use the more conservative  $T_{\text{eff}}$  and radius differences measured relative to the non-active stars (shown here as filled symbols and dashed lines).

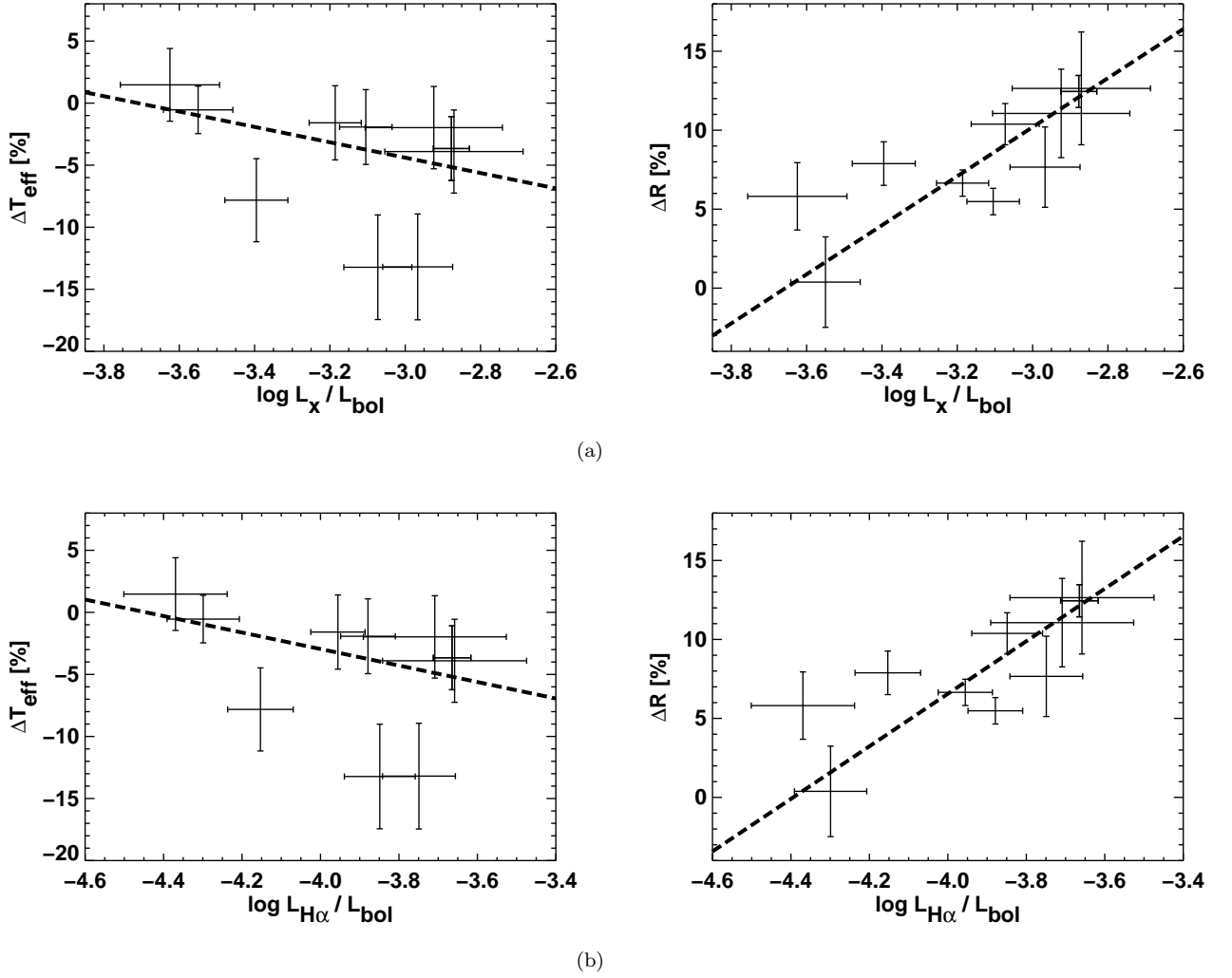


Fig. 4.— Suppression of effective temperatures (left) and inflation of radii (right) for low-mass eclipsing binaries from López-Morales (2007) as a function of fractional X-ray luminosity (a) and as a function of fractional H $\alpha$  luminosity (b). The  $\Delta T_{\text{eff}}$  and  $\Delta R$  are measured relative to the 3 Gyr isochrone of Baraffe et al. (1998). The fractional H $\alpha$  luminosities are based on the fractional X-ray luminosities, using the empirical X-ray-to-H $\alpha$  luminosity relation in Fig. 5. In all panels, the dashed line is a linear fit to the data.

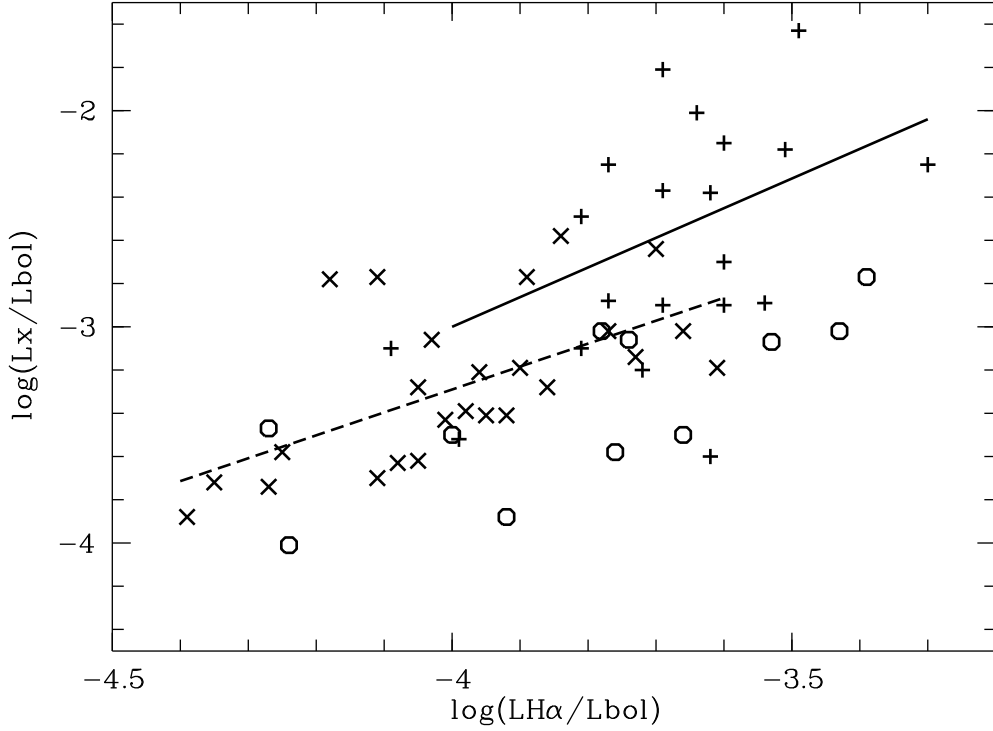


Fig. 5.— Fractional X-ray luminosity vs. fractional H $\alpha$  luminosity for low-mass star samples from field dwarfs (Delfosse et al. 1998, crosses), young stars Scholz et al. (2007, plus symbols), and field M-dwarfs (Reiners & Basri 2007, circles). Linear fits to the low-mass star samples are shown as solid (fit to plus symbols) and dashed (fit to crosses) lines.

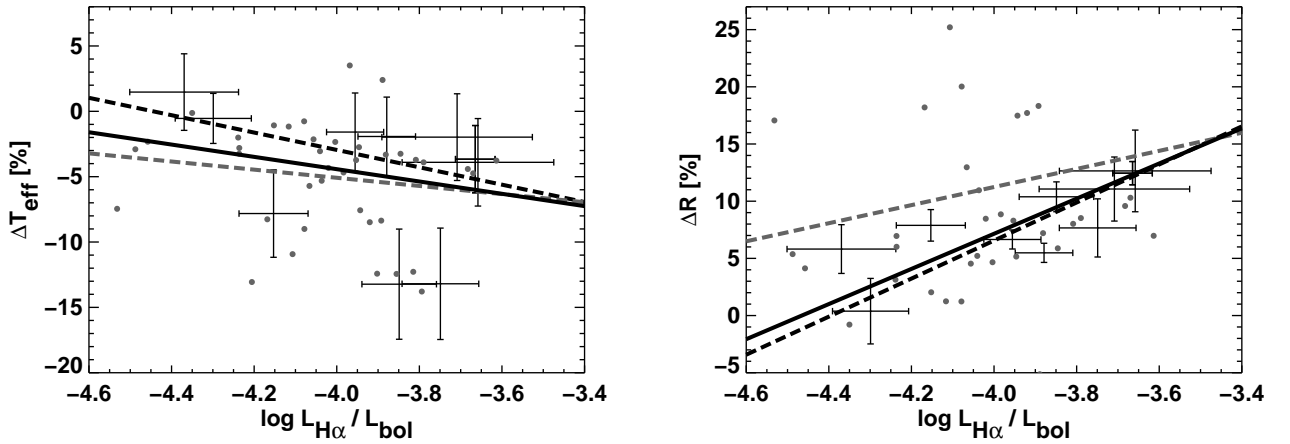


Fig. 6.— Temperature suppression (left) and radius inflation (right) as a function of fractional H $\alpha$  luminosity for both field M-dwarfs (filled symbols) and low-mass eclipsing binaries (error bars). Relations from Figs. 3(b) and 4(b) are reproduced (dashed lines). The final averaged best-fit relation in each panel is shown as a solid line. See Table 1 for the linear fit coefficients to these relations (Eqs. 1 and 2).

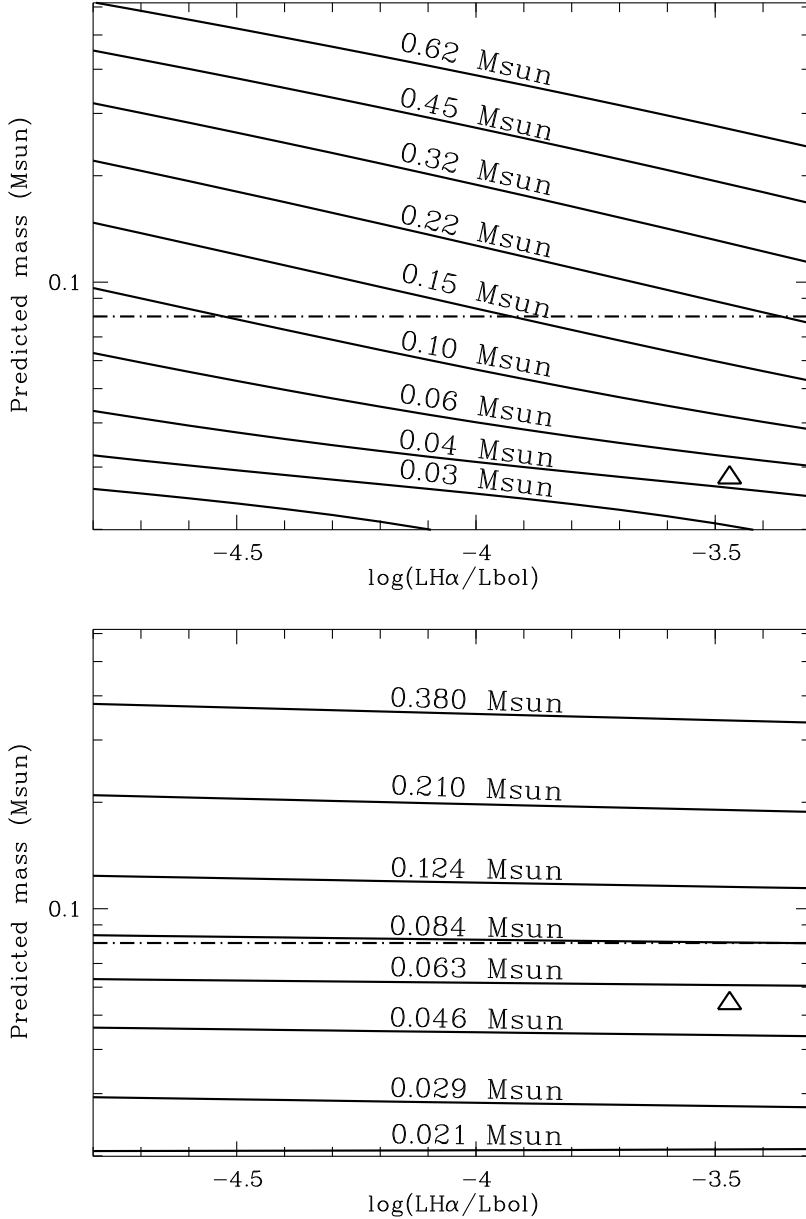


Fig. 7.— Inferred masses of low-mass stars and brown dwarfs as a function of  $L_{\text{H}\alpha}/L_{\text{bol}}$ , derived using the BCAH98 and DUSTY evolutionary tracks and the empirical relation between  $T_{\text{eff}}$  suppression and magnetic activity derived in this paper. In each panel, the true object masses are labelled on the curves, whereas the masses that would be inferred at a given activity level are shown on the ordinate. At low activity levels ( $\log L_{\text{H}\alpha}/L_{\text{bol}} \lesssim -4.6$ ), the inferred mass is close to the true mass. Top panel: Masses are inferred directly from the observed  $T_{\text{eff}}$ , which is susceptible to suppression at high activity levels, and therefore the inferred masses are systematically lower than the true masses. Bottom panel: Masses are inferred from the bolometric luminosity, estimated from the  $K$ -band absolute magnitude and bolometric correction (as would be appropriate for an object of known distance). Here the  $T_{\text{eff}}$  suppression effect enters only weakly via the  $T_{\text{eff}}$ -dependency of the  $K$ -band bolometric correction. The dash-dotted line in each panel shows the substellar limit. The triangle in each panel shows the position of the primary component in the eclipsing binary brown dwarf 2M0535–05, which has a true mass of  $0.06 M_{\odot}$ .